










## Article

# Ab Initio Investigation of the Stability, Electronic, Mechanical, and Transport Properties of New Double Half Heusler Alloys $\text{Ti}_2\text{Pt}_2\text{ZSb}$ ( $\text{Z} = \text{Al}, \text{Ga}, \text{In}$ )

Nurgul S. Soltanbek <sup>1</sup>, Nurpeiis A. Merali <sup>1,\*</sup>, Nursultan E. Sagatov <sup>2</sup>, Fatima U. Abuova <sup>1</sup>, Edgars Elsts <sup>3,\*</sup>, Aisulu U. Abuova <sup>1</sup>, Vladimir V. Khovaylo <sup>4</sup>, Talgat M. Inerbaev <sup>1,5</sup>, Marina Konuhova <sup>3</sup> and Anatoli I. Popov <sup>3</sup>

<sup>1</sup> Institute of Physical and Technical Sciences, L. N. Gumilyov Eurasian National University, Astana 010000, Kazakhstan; soltanbek\_ns\_2@enu.kz (N.S.S.); abuova\_fu@enu.kz (F.U.A.); abuova\_au@enu.kz (A.U.A.); inerbaev\_tm@enu.kz (T.M.I.)

<sup>2</sup> Sobolev Institute of Geology and Mineralogy, Siberian Branch of the Russian Academy of Sciences, Novosibirsk 630090, Russia; sagatovnye@igm.nsc.ru

<sup>3</sup> Institute of Solid-State Physics, University of Latvia, 1004 Riga, Latvia; marina.konuhova@cfi.lu.lv (M.K.); popov@latnet.lv (A.I.P.)

<sup>4</sup> Department of Functional Nanosystems and High-Temperature Materials, National University of Science and Technology "MISIS", Moscow 119049, Russia; khovaylo@misis.ru

<sup>5</sup> Vernadsky Institute of Geochemistry and Analytical Chemistry RAS, Moscow 119991, Russia

\* Correspondence: nurpeis\_m@enu.kz (N.A.M.); edgars.elsts@cfi.lu.lv (E.E.);

**Abstract:** This research aimed to explore the structural, electronic, mechanical, and vibrational properties of double half Heusler compounds with the generic formula  $\text{Ti}_2\text{Pt}_2\text{ZSb}$  ( $\text{Z} = \text{Al}, \text{Ga}, \text{and In}$ ), using density functional theory calculations. The generalized gradient approximation within the PBE functional was employed for structural relaxation and for calculations of vibrational and mechanical properties and thermal conductivity, while the hybrid HSE06 functional was employed for calculations of the electronic properties. Our results demonstrate that these compounds are energetically favorable and dynamically and mechanically stable. Our electronic structure calculations revealed that the  $\text{Ti}_2\text{Pt}_2\text{AlSb}$  double half Heusler compound is a non-magnetic semiconductor with an indirect band gap of 1.49 eV, while  $\text{Ti}_2\text{Pt}_2\text{GaSb}$  and  $\text{Ti}_2\text{Pt}_2\text{InSb}$  are non-magnetic semiconductors with direct band gaps of 1.40 eV. Further analysis, including phonon dispersion curves, the electron localization function (ELF), and Bader charge analysis, provided insights into the bonding character and vibrational properties of these materials. These findings suggest that double half Heusler compounds are promising candidates for thermoelectric device applications and energy-conversion devices, due to their favorable properties.

**Keywords:** double half Heusler alloy; mechanical properties; thermal conductivity; density functional theory



Received: 8 February 2025

Revised: 14 March 2025

Accepted: 15 March 2025

Published: 18 March 2025

**Citation:** Soltanbek, N.S.; Merali, N.A.; Sagatov, N.E.; Abuova, F.U.; Elsts, E.; Abuova, A.U.; Khovaylo, V.V.; Inerbaev, T.M.; Konuhova, M.; Popov, A.I. Ab Initio Investigation of the Stability, Electronic, Mechanical, and Transport Properties of New Double Half Heusler Alloys  $\text{Ti}_2\text{Pt}_2\text{ZSb}$  ( $\text{Z} = \text{Al}, \text{Ga}, \text{In}$ ). *Metals* **2025**, *15*, 329. <https://doi.org/10.3390/met15030329>

**Copyright:** © 2025 by the authors. Licensee MDPI, Basel, Switzerland. This article is an open access article distributed under the terms and conditions of the Creative Commons Attribution (CC BY) license (<https://creativecommons.org/licenses/by/4.0/>).

## 1. Introduction

Heusler alloys, characterized by their diverse transition metal elements (X, Y) and main group elements (Z), have emerged as promising materials for exploring novel electronic properties and multifunctional applications. While full ( $\text{X}_2\text{YZ}$ ) and half ( $\text{XYZ}$ ) Heusler alloys have been extensively studied [1–8], double Heusler alloys ( $\text{X}'\text{X}''\text{Y}_2\text{Z}_2$ ,  $\text{X}_2\text{Y}'\text{Y}''\text{Z}_2$ , and  $\text{X}_2\text{Y}_2\text{Z}'\text{Z}''$ ) have garnered significant interest in recent years, due to their unique combination of structural symmetry and electronic complexity [9,10]. The term 'double' emphasizes the doubling of the unit cell in comparison to their single-cell counterparts ( $\text{XYZ}$ ).

→  $X_2YY'Z_2$ ), where Y and Y' are aliovalent. In the quest for novel materials with tailored electronic properties and multifunctional capabilities, double half Heusler (DHH) alloys have emerged as compelling candidates for this role. With applications from spintronics to thermoelectrics, the study of DHH alloys has become a focal point in contemporary materials research because, compared to full and half Heusler compounds, double half Heusler alloys exhibit lower thermal conductivity and demonstrate excellent potential for thermoelectric applications [9,11,12].

Anand et al. [9] proposed that the thermal conductivity ( $\kappa$ ) in DHH compounds is primarily governed by reduced group velocity phonons and constrained by disorder scattering effects, which should reduce  $\kappa$  compared to contemporary ternary half Heusler thermoelectric materials, whose efficiency is hindered by their inherently high  $\kappa$ . Through the synthesis of  $Ti_2FeNiSb_2$ , they demonstrated and validated that this DHH alloy exhibits markedly lower thermal conductivity than its ternary half Heusler analog  $TiCoSb$ , thus presenting a superior foundation for the enhancement of thermoelectric efficiency [9]. Rached et al. [11] compared the structural, thermoelectric, and elastic properties of identical half Heusler ( $TiXSb$ , X = Ru, Pt) and DHH alloys ( $Ti_2RuPtSb_2$ ). The authors determined through computational analysis that the  $Ti_2RuPtSb_2$  compound exhibits pronounced peaks in the absorption coefficient within the ultraviolet (UV) spectral range, suggesting its potential utility for UV filters and UV photodetectors. The investigated materials also demonstrated promising thermoelectric properties, indicating their suitability as potential candidates for thermoelectric device applications [11,13–17]. In most instances, DHH alloys exhibit semiconductor behavior [18], exemplified by the investigations conducted by Bouhadjer et al. [12]. In their study,  $Ti_2FeNiSb_2$  and  $Ti_2Ni_2InSb$  alloys were observed, displaying band gap energies of 0.64 and 0.43 eV, respectively.

Ding et al. [19] devised a half-metallic DHH alloy,  $Mn_2FeCoSi_2$ , and they conducted an investigation into its electronic structure and magnetism. Additionally, they accurately examined the impact of atomic irregularities, encompassing six varieties of swap disorders and twelve varieties of antisite disorders, on the half-metallic properties of  $Mn_2FeCoSi_2$ . Transitioning to another study, Douinat et al. [20] explored the valence band contributions in two DHH alloys,  $Zr_2AlBiNi_2$  and  $Zr_2GaBiNi_2$ . They found that in both alloys the  $3d$  orbitals of Ni predominantly contribute to the valence band, while the conduction band is primarily influenced by the  $4d$  and  $3d$  orbitals of Zr and Ni, respectively. So, beyond thermoelectricity, DHH alloys demonstrate potential in spintronics, offering opportunities for spin injection, manipulation, and detection, which are essential to advancing electronic devices into the next generation [3]. Furthermore, extensive research has demonstrated the potential of double Heusler alloys in cutting-edge applications, including photovoltaics, ultraviolet (UV) sensing, solar cell technologies [21,22], and transportation [23–25].

Although numerous DHH alloys have been extensively studied over the past decade [26–30], a significant number of potential compound combinations remain unexplored, both experimentally and theoretically.

This paper presents a first-time investigation into the structural, electronic, mechanical, and phonon properties of the  $Ti_2Pt_2ZSb$  DHH compounds (where Z = Al, Ga, and In). The results obtained should enable a better understanding of their physicochemical properties, and an assessment of the potential suitability of the aforementioned alloys for thermoelectric devices and energy-conversion devices. This study differentiates itself from previous works by exploring and characterizing previously unreported compositions, thereby broadening the established domain of double half-Heusler materials.

## 2. Computational Methods

The calculations were performed using the Vienna Ab initio Simulation Package (VASP 5.4.4) within the density functional theory (DFT) methodology [31,32], which had previously been successfully used for calculations of other functional materials [33–37]. The generalized gradient approximation (GGA) within the Perdew–Burke–Ernzerhof functional (PAW) was utilized to account for the exchange–correlation interaction [38]. A baseline plane wave cutoff of 700 eV was applied in all instances. Integration of the Brillouin zone was achieved through a  $12 \times 12 \times 6$  k-point grid. These parameter choices demonstrated satisfactory convergence in total energy. The convergence tolerance for the calculations was set at a total energy difference within the range of  $10^{-7}$  eV/atom. The charge distribution on the ions was investigated by employing topological analysis, utilizing the Bader method. The phonon calculations were performed using the PhonoPy program (version 2.21.2) [39]. Real-space force constants were calculated using supercell and finite-displacement approaches, with  $2 \times 2 \times 1$  supercells for all the considered compounds. The elastic stiffness tensor ( $C_{ij}$ ) of the considered compounds was calculated using the stress ( $\sigma$ )–strain ( $\epsilon$ ) relation  $\sigma_i = C_{ij}\epsilon_j$ , and from the obtained data all the desired mechanical properties were estimated. Lattice thermal conductivity was calculated using a modified Debye–Callaway model, as implemented in AICON [40]. This approach uses the Debye temperature, phonon group velocity, and mode-resolved Gruneisen parameter as input, and it is especially appropriate for bulk crystalline materials.

## 3. Results

### 3.1. Structural Properties

Now, we present the obtained results for the new DHH compounds. DHH compounds are typically considered [9] to crystallize in a body-centered tetragonal structure belonging to the  $I\bar{4}2d$  space group (no. 122). An example of the crystal structure is shown in Figure 1. The X (Ti) and Y (Pt) atoms occupy the 8c and 8d sites, while the Z (Al, Ga, and In) and Z' (Sb) atoms occupy the 4a and 4b Wyckoff positions, respectively. The chosen X and Y atoms are transition metals, while the Z atom is an element of the main group. Table 1 provides an overview of the key attributes associated with these alloys:

**Table 1.** Structural data of considered  $\text{Ti}_2\text{Pt}_2\text{ZSb}$  compounds.

Compounds		$\text{Ti}_2\text{Pt}_2\text{AlSb}$	$\text{Ti}_2\text{Pt}_2\text{GaSb}$	$\text{Ti}_2\text{Pt}_2\text{InSb}$
Lattice parameter	$a = b$	6.120	6.121	5.905
	$c$	12.228	12.216	11.826
Coordinates		x	y	z
Atoms	Ti	0	0.5	0.495
	Pt	0.75	0.25	0.625
	Al/Ga/In	0	0.5	0.25
	Sb	0	0	0.5

Stable half Heusler semiconductor compounds adhere to the 18-valence electron counting (18-VEC) rule [41]. Alloys that conform to this rule exhibit notable stability and possess intriguing semiconductor properties, making them particularly relevant for various branches of physics.

DHH compounds are distinguished by their formation through the combination of 17- and 19-valence electron half Heusler compounds, resulting in stable 18-valence electron

structures. This transformation from ternary to quaternary compounds enables the creation of a diverse array of new alloys, suitable for a wide range of applications.

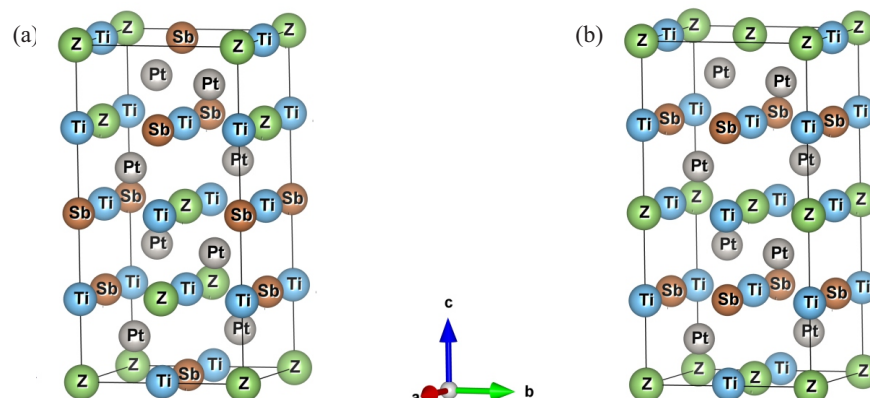


**Figure 1.** (a) Crystal structure of double half  $\text{Ti}_2\text{Pt}_2\text{ZSb}$  alloys ( $\text{Z} = \text{Al}, \text{Ga}, \text{In}$ ). (b) Crystal structure with alternating  $\text{Ti}/\text{Z}$  and  $\text{Ti}/\text{Sb}$  planes separated by half-filled  $\text{Pt}$  planes.

In our case, the DHH compound  $\text{Ti}_2\text{Pt}_2\text{AlSb}$ , which has 18 valence electrons, is considered to be a combination of the two half Heuslers:  $\text{TiPtAl}$  with 17 valence electrons and  $\text{TiPtSb}$  with 19 valence electrons. This rule also works for the other two  $\text{Ti}_2\text{Pt}_2\text{GaSb}$  and  $\text{Ti}_2\text{Pt}_2\text{InSb}$  double half Heusler compounds with 18 valence electrons. Accordingly, the chosen compounds should be considered stable. Therefore, we investigated the structures for energy, mechanical, and dynamic stability.

Based on the above, we considered whether the selected alloys were energetically favorable. The expected enthalpy of formation without correction for zero-point energy for the studied chemical compounds was calculated.

A formation enthalpy calculation was performed, using the following formula:

$$\Delta H_1(\text{X}_2\text{Y}_2\text{ZZ}') = H(\text{X}_2\text{Y}_2\text{ZZ}')/N - [2H(\text{X}) + 2H(\text{Y}) + H(\text{Z}) + H(\text{Z}')] ]$$

where  $N$  is the number of atoms in the chemical formula. The formation enthalpies of the  $\text{Ti}_2\text{Pt}_2\text{AlSb}$ ,  $\text{Ti}_2\text{Pt}_2\text{GaSb}$ , and  $\text{Ti}_2\text{Pt}_2\text{InSb}$  alloys were equal to  $-0.868$ ,  $-1.005$ , and  $-1.068$  eV/atom, respectively. The negative values of formation enthalpy indicate that these alloys are stable, relative to pure  $\text{Ti}$ ,  $\text{Pt}$ ,  $\text{Z}$  ( $\text{Z} = \text{Al}, \text{Ga}, \text{In}$ ) and  $\text{Sb}$ . To evaluate the energetic preference of the DHH phase against potential phase separation into two neighboring half Heusler compounds, the enthalpies of  $\text{TiPtZ}$  ( $\text{Z} = \text{Al}, \text{Ga}, \text{In}$ ) and  $\text{TiPtSb}$  were calculated and compared with that of  $\text{Ti}_2\text{Pt}_2\text{ZSb}$ :

$$\Delta H_2(\text{Ti}_2\text{Pt}_2\text{AlSb}) = H(\text{Ti}_2\text{Pt}_2\text{AlSb}) - [H(\text{TiPtAl}) + H(\text{TiPtSb})] = -0.098 \text{ eV/atom}$$

$$\Delta H_2(\text{Ti}_2\text{Pt}_2\text{GaSb}) = H(\text{Ti}_2\text{Pt}_2\text{GaSb}) - [H(\text{TiPtGa}) + H(\text{TiPtSb})] = -0.085 \text{ eV/atom}$$

$$\Delta H_2(\text{Ti}_2\text{Pt}_2\text{InSb}) = H(\text{Ti}_2\text{Pt}_2\text{InSb}) - [H(\text{TiPtIn}) + H(\text{TiPtSb})] = -0.106 \text{ eV/atom}$$

These negative values, which are greater than  $kT$ , indicate that  $\text{Ti}_2\text{Pt}_2\text{ZSb}$  ( $\text{Z} = \text{Al}, \text{Ga}, \text{In}$ ) DHH compounds remain energetically favorable compared to decomposition into two half Heusler phases. While we acknowledge that this does not fully rule out alternative phase formations, our results suggest that the single-phase DHH structure is energetically competitive.

In addition, we constructed a structure in which  $\text{Ti}-\text{Z}$  planes alternated with a half-filled  $\text{Pt}$  plane, followed by a  $\text{Ti}/\text{Sb}$  plane, another half-filled  $\text{Pt}$  plane, and, again, a  $\text{Ti}/\text{Z}$  plane, and so on, as shown in Figure 1b. With this arrangement of atoms, the symmetry

of the structure was reduced to  $P\bar{4}m2$ . The formation enthalpy of the structure was found to be  $-0.85$  eV/atom. In comparison, it was evident that the traditionally proposed DHH structure ( $I\bar{4}2m$ ) was more energetically favorable than the  $P\bar{4}m2$  structure.

As expected from the 18-valence electron counting rule, the studied alloys were found to be energetically stable. It is worth noting the presence of these DHH alloys (in the form of the  $I\bar{4}2m$  structure) in the Open Quantum Materials Database (OQMD), where they are listed as stable. Nevertheless, no experimental or theoretical studies of these DHH compounds have been published to date. Our calculated formation enthalpies are consistent with the OQMD data, indicating that our calculations are valid.

### 3.2. Vibrational Properties

The vibrational properties of the material were analyzed, to describe the dynamic stability. The phonon dispersion curves and phonon density of states of the  $\text{Ti}_2\text{Pt}_2\text{ZSb}$  alloys are shown in Figure 2. The results of the phonon dispersion curves are displayed in the first Brillouin zone. Since all three compounds have 12 atoms in the primitive cell, there are 36 vibrational modes in the phonon band structure with the following mechanical representation,  $M = 2A_1 + 3A_2 + 4B_1 + 5B_2 + 11E$ . The first three acoustic modes ( $\Gamma_{\text{acoustic}} = B_2 + E$ ) represent the movement of the center of mass, while the optical modes ( $\Gamma_{\text{optic}} = 2A_1 + 3A_2 + 4B_1 + 4B_2 + 10E$ ) characterize the relative motion between atoms. According to a group theoretical analysis, there are 30 Raman active ( $\Gamma_{\text{Raman}} = 2A_1 + 4B_1 + 4B_2 + 10E$ ), 24 IR active ( $\Gamma_{\text{IR}} = 4B_2 + 10E$ ), and 3 silent ( $\Gamma_{\text{Silent}} = 3A_2$ ) modes for  $\text{Ti}_2\text{Pt}_2\text{ZSb}$  compounds. The calculated vibrational modes at  $\Gamma$ -point are presented in Table 2.

**Table 2.** Calculated optical modes ( $\omega$ ) of  $\text{Ti}_2\text{Pt}_2\text{ZSb}$  ( $Z = \text{Al, Ga, and In}$ ), their activity, and their corresponding Mulliken symbols.

Mulliken Symbol	Activity	$\omega$ , THz		
		$\text{Ti}_2\text{Pt}_2\text{AlSb}$	$\text{Ti}_2\text{Pt}_2\text{GaSb}$	$\text{Ti}_2\text{Pt}_2\text{InSb}$
$E$	Raman, IR	2.700	2.644	2.322
$E$	Raman, IR	3.023	2.750	2.322
$B_1$	Raman	3.158	3.049	2.768
$B_2$	Raman, IR	3.287	3.116	2.732
$A_2$	Silent	3.666	3.672	3.671
$A_1$	Raman	3.678	3.674	3.658
$A_2$	Silent	4.147	4.192	4.125
$E$	Raman, IR	4.312	4.127	3.759
$B_1$	Raman	4.704	4.318	3.763
$E$	Raman, IR	4.848	4.749	4.615
$B_2$	Raman, IR	5.251	5.358	5.163
$E$	Raman, IR	5.874	4.949	4.862
$E$	Raman, IR	6.162	5.334	5.198
$B_2$	Raman, IR	6.512	5.544	5.411
$B_1$	Raman	6.587	5.572	5.406
$E$	Raman, IR	7.295	6.330	6.010
$A_1$	Raman	7.414	7.269	6.750
$A_2$	Silent	7.433	7.265	6.756
$E$	Raman, IR	7.952	6.953	6.946
$E$	Raman, IR	8.874	7.991	7.079
$B_2$	Raman, IR	8.914	6.625	6.059
$E$	Raman, IR	9.634	8.231	7.323
$B_1$	Raman	9.783	7.824	7.523

Analyzing the phonon density of states, it can be seen that for all three compounds in the frequency from 0 to 4 THz, the main contribution to the acoustic modes corresponded to Pt atoms, while from 4 to 6 THz the main contribution to the acoustic modes corresponded

to Sb atoms. For  $\text{Ti}_2\text{Pt}_2\text{GaSb}$  and  $\text{Ti}_2\text{Pt}_2\text{InSb}$  alloys in the frequency  $\approx 5.5\text{--}6.2\text{ THz}$ , a phonon band gap was observed. Conversely,  $\text{Ti}_2\text{Pt}_2\text{AlSb}$  exhibited two smaller phonon band gaps in the frequencies  $\approx 7.3\text{--}7.4\text{ THz}$  and  $\approx 8.1\text{--}8.5\text{ THz}$ . Additionally, a fifth phonon band gap with frequencies exceeding  $9\text{ THz}$  was observed, primarily influenced by the vibrations of the lighter aluminum atoms.

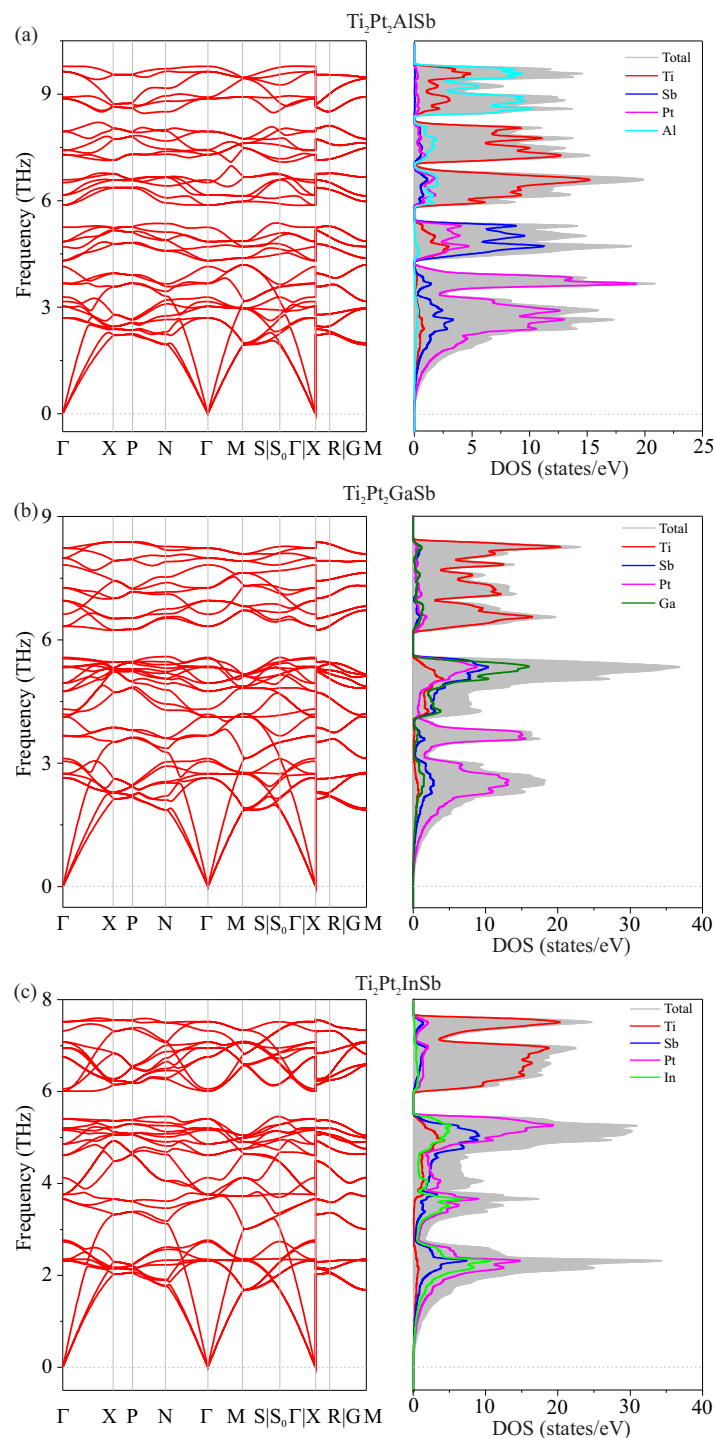


**Figure 2.** Calculated phonon dispersion curves and phonon density of states for (a)  $\text{Ti}_2\text{Pt}_2\text{AlSb}$ , (b)  $\text{Ti}_2\text{Pt}_2\text{GaSb}$ , (c)  $\text{Ti}_2\text{Pt}_2\text{InSb}$  compounds.

According to the performed calculation of the phonon dispersion, no imaginary modes in the whole Brillouin zone were found, which means that when the system was perturbed



the atoms returned to their equilibrium positions. This fact proves that the considered alloys are dynamically stable.

### 3.3. Elastic Properties

The number of independent elastic constants usually depends on the symmetry of the structure under investigation. In our case, for a tetragonal crystal structure, there were six independent elastic constants,  $C_{11}$ ,  $C_{12}$ ,  $C_{13}$ ,  $C_{33}$ ,  $C_{44}$ ,  $C_{66}$ . Table 3 contains the calculated elastic constants  $C_{ij}$  for all three compounds. A compound that satisfies the Born–Huang condition can be considered mechanically stable [42]. Four principal criteria must be satisfied by our system:

$$\begin{cases} C_{11} > |C_{12}|, \\ 2C_{13}^2 < C_{33}(C_{11} + C_{12}), \\ C_{44} > 0, \\ C_{66} > 0 \end{cases}$$

Based on the calculations, all three alloys met the required conditions and could be considered mechanically stable. Considering the above, the  $\text{Ti}_2\text{Pt}_2\text{ZSb}$  alloys were tested for energy, dynamic, and mechanical stability. They were found to be stable according to all three criteria.

Realizing that the elastic constants  $C_{11}$  and  $C_{33}$  demonstrated compression resistance, while the constants  $C_{12}$ ,  $C_{13}$ ,  $C_{44}$ , and  $C_{66}$  showed shear resistance, from the information in Table 3 the compression resistance of  $\text{Ti}_2\text{Pt}_2\text{ZSb}$  alloys was larger than the resistance to one-dimensional shear deformations. Utilizing the known elastic constants  $C_{ij}$  above, the elastic moduli as shear, bulk, Young's modulus, and Poisson's ratio could be estimated. The bulk modulus of elasticity  $B$  served as an indicator of the material's resistance to uniform compression. The shear modulus  $G$  characterized the material's resistance to shear deformations. The upper and lower boundaries of the actual polycrystalline constants were described by the Voigt [43] and Reuss [44] equations; for a tetragonal crystal, they could be approximated, using the Voigt average ( $B_V, G_V$ ) and Reuss' modulus ( $B_R, G_R$ ) derived from the elastic constants. Taking into consideration Hill's recommendations [45,46], the estimation of the volume and shear modulus was the arithmetic mean of the upper and lower limits, and the following equations were used:

$$B_V = \frac{2(C_{11} + C_{12}) + C_{33} + 4C_{13}}{9}$$

$$G_V = \frac{M + 3C_{11} - 3C_{12} + 12C_{44} + 6C_{66}}{30}$$

$$B_R = \frac{(C_{11} + C_{12})C_{33} - 2C_{13}^2}{M}$$

$$G_R = 15 \left/ \left\{ \frac{18B_V}{C^2} + \left[ \frac{6}{(C_{11} - C_{12}) + \left(\frac{6}{C_{44}}\right) + \left(\frac{3}{C_{66}}\right)} \right] \right\} \right.$$

where  $C^2 = (C_{11} + C_{12})C_{33} - C_{13}^2$ ;  $M = C_{11} + C_{12} + 2C_{33} - 3C_{13}$ ;

$$B = \frac{B_V + B_R}{2}; \quad G = \frac{G_V + G_R}{2}$$

**Table 3.** Calculated elastic constants  $C_{ij}$  for  $\text{Ti}_2\text{Pt}_2\text{ZSb}$  compounds ( $\text{Z} = \text{Al, Ga, and In}$ ) in GPa.

Compounds	$C_{11}$	$C_{12}$	$C_{13}$	$C_{33}$	$C_{44}$	$C_{66}$
$\text{Ti}_2\text{Pt}_2\text{AlSb}$	199.6	111.5	108.6	196.5	69.1	68
$\text{Ti}_2\text{Pt}_2\text{GaSb}$	194.2	115.2	113.5	191.7	66.9	66.9
$\text{Ti}_2\text{Pt}_2\text{InSb}$	191.3	106.6	106.9	188.8	58.6	59

The calculated  $B$ ,  $G$ ,  $E$ , and  $\nu$  are presented in Table 4. Upon analyzing the bulk modulus, the  $\text{Ti}_2\text{Pt}_2\text{GaSb}$  alloy exhibited the highest resistance to uniform compression among the three alloys, while  $\text{Ti}_2\text{Pt}_2\text{InSb}$  showed the lowest resistance. Notably, the shear modulus decreased as the ionic radius of the constituent elements increased, implying that larger ionic radii contribute to reduced resistance to shear stress.

Young's modulus indicates the stiffness of a material. The Young's modulus equation can be written as follows:  $E = \frac{9BG}{3B+G}$  [47]. Poisson's ratio shows the measure of deformation in one direction under the action of stress applied in a perpendicular direction [48]. In our case, for a tetragonal system, it was determined by the following relation:  $\nu = \frac{3B-2G}{2(3B+G)}$  [49]. High  $E$  values correspond to very stiff materials with strong covalent bonds. It is clear from Table 4 that Young's modulus decreased with increasing ionic radius, while, on the contrary, the Poisson's ratio increased. These values typically indicate materials with metal compounds and are close to the typical range for metals and ductile materials. Simply put, with an increase in the radius of the  $\text{Z}$  atom, the stiffness of the material decreases, but, at the same time, it maintains a balance between strength and plasticity: the material can deform but retain its shape.

Table 4 also shows values such as fracture toughness, Vickers hardness, and the brittleness of the material. Based on our calculations, the Vickers hardness  $H_V$  for the  $\text{Ti}_2\text{Pt}_2\text{InSb}$  alloy is the lowest and equals 4.2 GPa.  $\text{Ti}_2\text{Pt}_2\text{AlSb}$  has the highest value of  $H_V$  (5.3 GPa), while  $\text{Ti}_2\text{Pt}_2\text{GaSb}$  has an intermediate value of  $H_V$  (4.5 GPa). To calculate the Vickers hardness of the alloys under investigation, we used the empirical models proposed by Chen [50]  $H_V^{\text{Chen}} = 2 \cdot (k^2 \cdot G)^{0.585} - 3$  and Tian [51]  $H_V^{\text{Tian}} = 0.92 \cdot k^{1.137} \cdot G^{0.708}$ , where  $k = G/B$ . In our study,  $H_V$  was calculated as the average value obtained from  $H_V^{\text{Chen}}$  and  $H_V^{\text{Tian}}$ :  $H_V = \frac{H_V^{\text{Chen}} + H_V^{\text{Tian}}}{2}$ . Fracture toughness can be described as the resistance of a material to cracks and fractures when exposed to external forces. To calculate fracture toughness, we used the following relation:

$$K_{IC} = V_0^{1/6} \cdot G \cdot \left(\frac{B}{G}\right)^{1/2}$$

where  $V_0$  is the volume per atom (in  $\text{m}^3/\text{atom}$ ) [52]. As for fracture toughness  $K_{IC}$ , this decreases with the increasing ionic radius of the  $\text{Z}$  atom in the  $\text{Ti}_2\text{Pt}_2\text{ZSb}$  alloy.

Using the calculated bulk and shear moduli, the percentages of elastic anisotropy for the bulk modulus  $A_B$  and shear modulus  $A_G$  were calculated. For elastic isotropy, the value corresponded to 0%, while the maximum possible anisotropy corresponded to a value of 100%. A comparative analysis of the elastic properties of double half Heusler alloys and their half Heusler analogue showed that aliovalent substitution had a negligible effect on the values of the elastic moduli. It should be noted that the calculated mechanical properties (especially  $H_V$ ,  $K_{IC}$ ) represented theoretical approximations rather than definitive results. In some cases, their applicability may be limited [53]. Therefore, these calculations should be interpreted with consideration of their inherent limitations.



**Table 4.** Calculated values of the bulk (in GPa), shear (in GPa), Young’s (in GPa) moduli, Poisson’s ratio, Vickers hardness (in GPa), fracture toughness (in  $\text{MPa m}^{1/2}$ ), bulk and shear anisotropy factors (%), and melting temperature (in K) of  $\text{Ti}_2\text{Pt}_2\text{ZSb}$  ( $\text{Z} = \text{Al, Ga, In}$ ) double half Heusler compounds, and comparison with  $\text{TiPtSn}$  [54].

Compounds	$B$	$G$	$E$	$\nu$	$H_V$	$K_{IC}$	$A_B$	$A_G$
$\text{Ti}_2\text{Pt}_2\text{AlSb}$	139	58	152	0.318	5.3	2.5	0.01	2.26
$\text{Ti}_2\text{Pt}_2\text{GaSb}$	140	54	144	0.329	4.5	2.4	0.01	3.25
$\text{Ti}_2\text{Pt}_2\text{InSb}$	135	51	136	0.331	4.2	2.3	0.01	1.38
$\text{TiPtSn}$	146	57	150	0.329	4.7	–	0.00	1.72

### 3.4. Thermal Conductivity

The lattice thermal conductivity was calculated and is illustrated in Figure 3. The calculated values of the lattice thermal conductivity  $\kappa_L$  ( $\text{W}/(\text{m}\cdot\text{K})$ ), the longitudinal sound velocity  $v_l$  ( $\text{m/s}$ ), the transverse sound velocity  $v_t$  ( $\text{m/s}$ ), and the average sound velocity  $v_{ave}$  ( $\text{m/s}$ ) of the  $\text{Ti}_2\text{Pt}_2\text{ZSb}$  DHH compounds with  $\text{TiPtSn}$  are presented in Table 5. The sound velocities for  $\text{TiPtSn}$  were recalculated using the  $C_{ij}$  constants provided in [54]. It can be seen that with increasing temperature the lattice thermal conductivity for all three double half Heusler alloys decreased gradually. At 300 K, the lattice thermal conductivity for the  $\text{Ti}_2\text{Pt}_2\text{AlSb}$  compound was  $2.67 \text{ W}/(\text{m}\cdot\text{K})$ , for  $\text{Ti}_2\text{Pt}_2\text{GaSb}$  it was  $2.52 \text{ W}/(\text{m}\cdot\text{K})$ , and for the  $\text{Ti}_2\text{Pt}_2\text{InSb}$  compound it was  $2.35 \text{ W}/(\text{m}\cdot\text{K})$ . A comparison between the investigated DHH alloys and their analogue  $\text{TiPtSn}$  indicated that aliovalent substitution of Sn leads to an increase in lattice thermal conductivity by approximately threefold. In the case of sound velocities, their values did not differ significantly. In comparison to the  $\text{MgZrNi}_2\text{Bi}_2$ ,  $\text{MgZrNi}_2\text{Sb}_2$ ,  $\text{Zr}_2\text{Ni}_2\text{GaBi}$ , and  $\text{Ti}_2\text{FeNiSb}_2$  DHH alloys, for which the lattice thermal conductivity at 300 K is approximately  $5\text{--}7 \text{ W}/(\text{m}\cdot\text{K})$  [9], the alloys investigated in this study exhibited significantly lower lattice thermal conductivity, which was comparable to the thermal conductivity of the conventional thermoelectric material  $\text{PbTe}$ , approximately  $2.3 \text{ W}/(\text{m}\cdot\text{K})$  at 300 K [55,56].

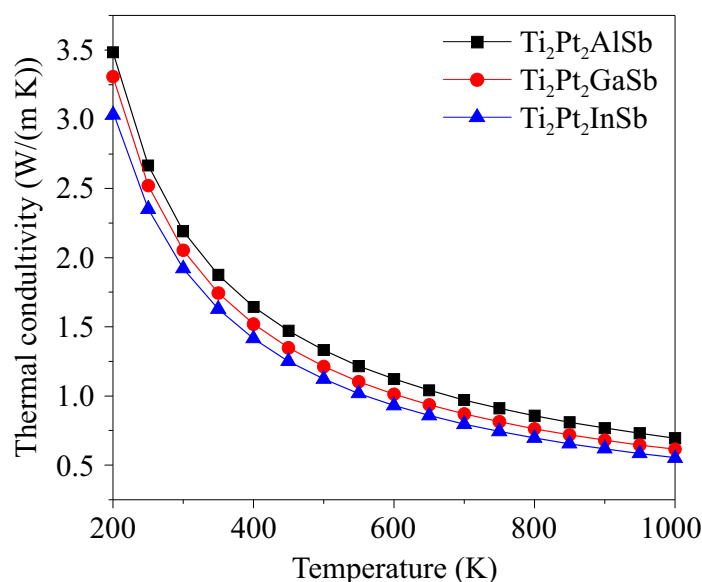


**Figure 3.** Lattice thermal conductivity  $\kappa_L$  of  $\text{Ti}_2\text{Pt}_2\text{ZSb}$  ( $\text{Z} = \text{Al, Ga, In}$ ) at different temperatures, ranging from 200 K to 1000 K.

**Table 5.** The calculated lattice thermal conductivity  $\kappa_L$  (W/(m·K), longitudinal sound velocity  $v_l$  (m/s), transverse sound velocity  $v_t$  (m/s), and average sound velocity  $v_{ave}$  (m/s) for  $\text{Ti}_2\text{Pt}_2\text{ZSb}$  (Z = Al, Ga, and In) and comparison with  $\text{TiPtSn}$ .

Compounds	$\kappa_L$	$v_l$	$v_t$	$v_{ave}$	Ref.
$\text{Ti}_2\text{Pt}_2\text{AlSb}$	2.67	4847	2505	2911	this study
$\text{Ti}_2\text{Pt}_2\text{GaSb}$	2.52	4653	2349	2732	this study
$\text{Ti}_2\text{Pt}_2\text{InSb}$	2.35	4523	2273	2661	this study
$\text{TiPtSn}$	9.2	4553	2569	2924	[57]

### 3.5. Electronic Properties

The electronic properties of the materials were investigated by calculating the density of states and the band structure, using density functional theory (DFT). Since it is known that standard DFT functionals greatly underestimate the band gap, the HSE06 hybrid functional [58] was used to estimate the band structure and density of states (DOS). The density of states is an essential factor in characterizing energy levels. The calculated band structure and DOS are shown in Figure 4.

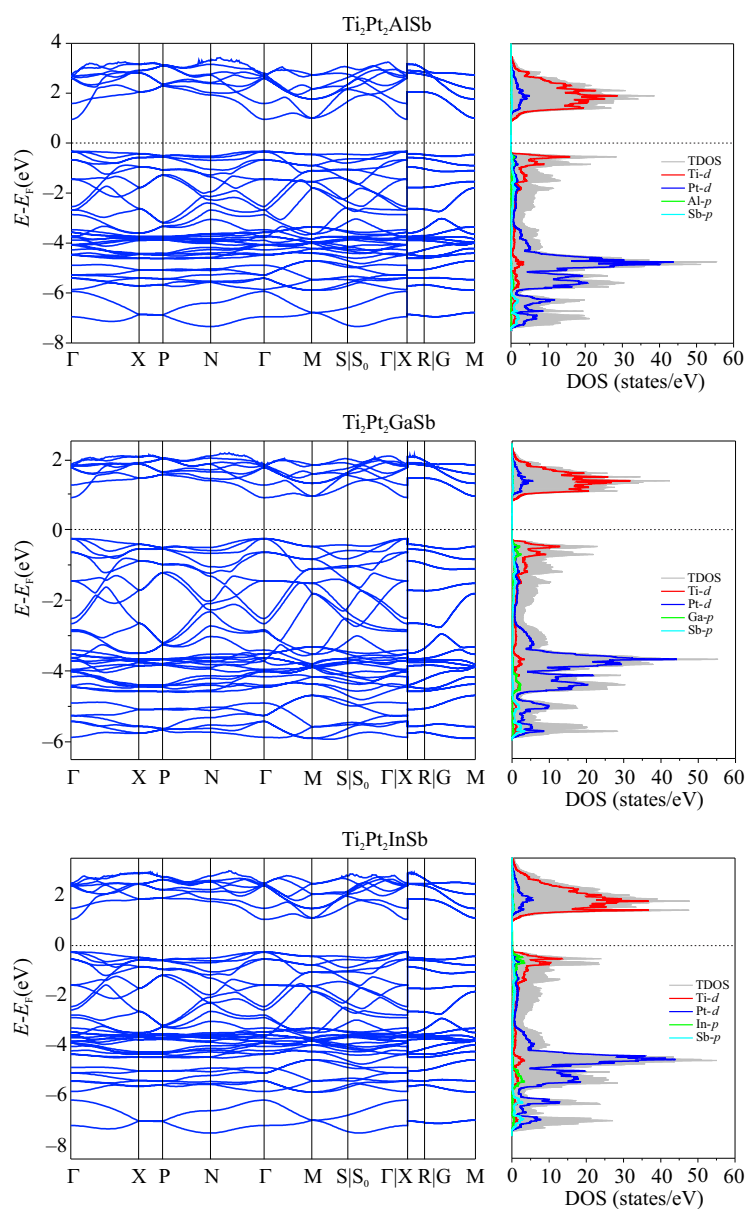


**Figure 4.** The density of states and electronic band structure of the  $\text{Ti}_2\text{Pt}_2\text{ZSb}$  double half Heusler alloys.

Analysis of the DOS and band structure revealed the presence of a band gap proximate to the Fermi level, with respective values of 1.43 eV (indirect) for the  $\text{Ti}_2\text{Pt}_2\text{AlSb}$  alloy and 1.40 eV (direct) for the  $\text{Ti}_2\text{Pt}_2\text{GaSb}$  and  $\text{Ti}_2\text{Pt}_2\text{InSb}$  alloys. According to the results obtained, the maximum of the valence band (VBM) lay at the  $\Gamma$ -point and the minimum of the conduction band (CBM) at the M-point. The band profiles were alike for all three compounds. For comparison, the band gap of the 18-valence electron analogue  $\text{TiPtSn}$  was reported to be 1.31 eV [59].

Our analysis of the three graphs shows that Pt  $d$  states made a predominant contribution to the total density of states at the bottom of the valence band, from  $\approx -5.5$  to  $-2.5$  eV, whereas at the top of the conduction band, from  $\approx 1$  to 2 eV, the unoccupied Ti  $d$  states made the most significant contribution. Furthermore, near the Fermi level, the contribution of indium In  $p$  states among the Z atoms was significantly greater than that of the Al  $p$  states. Proximal to the Fermi level, at the valence band maximum, contributions from all atomic species are observable, with the occupied  $d$  states of Ti exerting the most significant influence.

The results of the electronic characteristics of the DHH alloys determined that the chosen alloys exhibit properties of non-magnetic direct band gap semiconductors.

Furthermore, a Bader analysis was conducted, to ascertain the atomic charges, as shown in Table 6. This analysis enabled a detailed understanding of the charge distribution within the studied compounds. The Bader charges of the Ti atoms decreased slightly as the Z element changed from Al to In. This trend indicates a gradual increase in charge delocalization and a slight reduction in the ionic character of Ti with heavier Z elements.

**Table 6.** Bader charges of atoms ( $e$ ) in  $\text{Ti}_2\text{Pt}_2\text{ZSb}$  (Z = Al, Ga, In) alloys.

Compounds	Ti	Pt	Z	Sb
$\text{Ti}_2\text{Pt}_2\text{AlSb}$	+1.99	−3.59	+3	+0.20
$\text{Ti}_2\text{Pt}_2\text{GaSb}$	+1.98	−3.62	+3	+0.28
$\text{Ti}_2\text{Pt}_2\text{InSb}$	+1.94	−3.63	+3	+0.40

In case of the Pt atoms, the increasing negative charge suggests that there was an enhanced electron transfer to the Pt atoms as the atomic size of the Z element increased, likely due to the influence of bonding and electronegativity differences. The Sb atoms showed an increasing trend in Bader charges. This trend correlated with an increasing covalent character or electron density redistribution towards Sb as the Z element became heavier. The Z element retained a constant Bader charge of  $(+3e)$  across all the compounds. This uniformity suggests that Z elements contribute primarily through their stable valence state, with minimal variation in charge transfer dynamics. To illustrate the various interactions and chemical bonds in the selected DHH alloys, the electronic localization function (ELF) was calculated. Figure 5 depicts the electronic localization function data for  $\text{Ti}_2\text{Pt}_2\text{AlSb}$ ,  $\text{Ti}_2\text{Pt}_2\text{GaSb}$ , and  $\text{Ti}_2\text{Pt}_2\text{InSb}$ . High values of the ELF between atoms indicate regions where electrons tended to pair, reflecting the covalent bonding character between the nearest-neighbor atoms in the compounds. As can be seen from Figure 5, the charge accumulation occurred halfway through each Sb–Pt vector, and the maximum ELF value between the Sb and Pt atoms was about 0.4, which is indicative of ionic bonding. In contrast, the bond between the Z atoms (Al, Ga, In) and the Pt atoms predominantly exhibited a covalent nature, with the ELF values reaching 0.8. Moreover, as the ionic radius of the Z atom increased (Al–Ga–In), the covalent character of the bond between Pt and Z atoms was enhanced. The comparison of the ELF for the selected alloys shows that the nature of the electron density distribution was mainly determined by the nature of the element Z.

However, the overall pattern of the electron density distribution remained qualitatively similar for all the selected alloys, which indicates the similarity of their electronic structure.

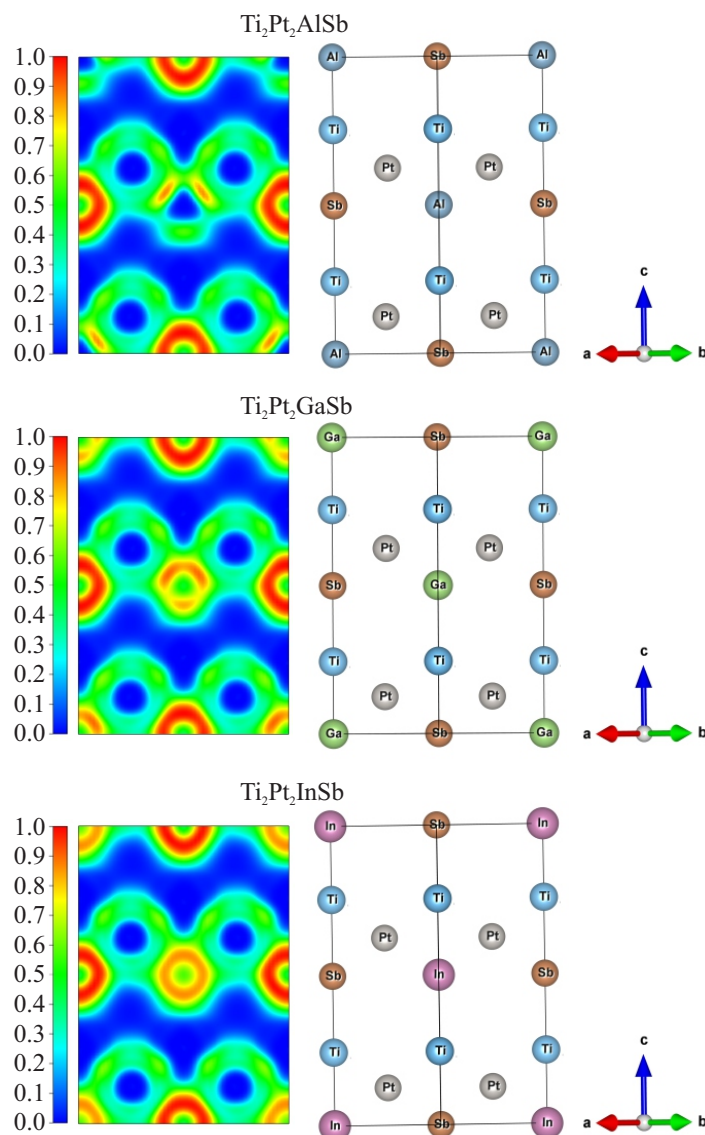


**Figure 5.** Calculates the ELF of the  $\text{Ti}_2\text{Pt}_2\text{ZSb}$  double half Heusler alloys in the (110) plane.

#### 4. Conclusions

In this study, we conducted a first-principles investigation of the structural, electronic, vibrational, and mechanical properties and the thermal conductivity of  $\text{Ti}_2\text{Pt}_2\text{ZSb}$  ( $\text{Z} = \text{Al}, \text{Ga}, \text{and In}$ ) double half Heusler compounds. Our findings confirm that all three compounds are energetically, dynamically, and mechanically stable, indicating their feasibility for experimental synthesis. The electronic structure analysis revealed semiconducting behavior, with  $\text{Ti}_2\text{Pt}_2\text{AlSb}$  exhibiting an indirect band gap (1.43 eV), while  $\text{Ti}_2\text{Pt}_2\text{GaSb}$  and  $\text{Ti}_2\text{Pt}_2\text{InSb}$  had direct band gaps (1.40 eV) of similar magnitude. Our phonon dispersion analysis confirmed their vibrational stability, while the electron localization function (ELF) and our Bader charge analysis provided insights into the nature of the chemical bonding. Our Bader charge analysis provided further insight into electronic charge interactions, enhancing our understanding of the influence of electronic structure on material properties. These findings contribute valuable insights into developing robust, high-performance materials for thermoelectric (energy-conversion) devices. Overall, these results contribute to a deeper

understanding of the fundamental properties of double half Heusler alloys and may guide future experimental and theoretical research in exploring their functional applications.

**Author Contributions:** Conceptualization N.S.S., N.A.M. and T.M.I.; Methodology, V.V.K.; Software, A.U.A. and T.M.I.; Validation, N.E.S., E.E., A.U.A., V.V.K. and T.M.I.; Formal analysis, N.E.S.; Investigation, N.S.S., N.A.M. and F.U.A.; Resources, E.E., M.K. and A.I.P.; Data curation, N.S.S., N.A.M., F.U.A. and A.U.A.; Writing—original draft, N.S.S. and N.A.M.; Writing—review & editing, N.S.S., N.A.M., N.E.S. and T.M.I.; Visualization, T.M.I.; Supervision, V.V.K. and T.M.I.; Funding acquisition, M.K. and A.I.P. All authors have read and agreed to the published version of the manuscript.

**Funding:** This study was funded by the Ministry of Science and Higher Education of the Republic of Kazakhstan under the “Zhas Galym” project for 2024–2026 AP22683528 “Computer design of thermoelectric and spintronic materials based on Heusler alloys”, and V.V.K. acknowledges the Priority-2030 program of NUST MISIS, grant K2-2022-022. The calculations were performed using resources provided by the Novosibirsk State University Supercomputer Center. N.E.S. was supported by the state assignment of IGM SB RAS (122041400176-0). The work by T.M.I. was carried out within the state assignment of the Vernadsky Institute of Geochemistry and Analytical Chemistry of the Russian Academy of Sciences (GEOKHI RAS). In addition, M.K. and A.I.P. were supported by the EUROfusion Enabling Research Project ENR-MAT.02. ISSP-UL-“New dielectric functional materials and interfaces (DFMI)—Theoretical and Experimental analysis.” This work has been carried out within the framework of the EUROfusion Consortium, funded by the European Union via the Euratom Research and Training Programme (Grant Agreement No. 101052200—EUROfusion). The views and opinions expressed are, however, those of the author(s) only and do not necessarily reflect those of the European Union or the European Commission, and neither the European Union nor the European Commission can be held responsible for them.

**Data Availability Statement:** The original contributions presented in the study are included in the article, further inquiries can be directed to the corresponding authors.

**Conflicts of Interest:** The authors declare no conflict of interest.

## References

1. Webster, P.J. Heusler alloys. *Contemp. Phys.* **1969**, *10*, 559–577. [\[CrossRef\]](#)
2. Tavares, S.; Yang, K.; Meyers, M.A. Heusler alloys: Past, properties, new alloys, and prospects. *Prog. Mater. Sci.* **2023**, *132*, 101017. [\[CrossRef\]](#)
3. Elphick, K.; Frost, W.; Samiepour, M.; Kubota, T.; Takanashi, K.; Sukegawa, H.; Mitani, S.; Hirohata, A. Heusler alloys for spintronic devices: Review on recent development and future perspectives. *Sci. Technol. Adv. Mater.* **2021**, *22*, 235–271. [\[CrossRef\]](#)
4. Rogl, G.; Grytsiv, A.; Gürth, M.; Tavassoli, A.; Ebner, C.; Wünschek, A.; Puchegger, S.; Soprunyuk, V.; Schranz, W.; Bauer, E.; et al. Mechanical properties of half-Heusler alloys. *Acta Mater.* **2016**, *107*, 178–195. [\[CrossRef\]](#)
5. Abuova, A.; Merali, N.; Abuova, F.; Khovaylo, V.; Sagatov, N.; Inerbaev, T. Electronic properties and chemical bonding in V<sub>2</sub>FeSi and Fe<sub>2</sub>VSi Heusler alloys. *Crystals* **2022**, *12*, 1546. [\[CrossRef\]](#)
6. Abuova, F.; Inerbaev, T.; Abuova, A.; Merali, N.; Soltanbek, N.; Kaptagay, G.; Seredina, M.; Khovaylo, V. Structural, electronic, and magnetic properties of Mn<sub>2</sub>Co<sub>1-x</sub>VXZ (Z = Ga, Al) Heusler alloys: An insight from DFT study. *Magnetochemistry* **2021**, *7*, 159. [\[CrossRef\]](#)
7. Casper, F.; Graf, T.; Chadov, S.; Balke, B.; Felser, C. Half-Heusler compounds: Novel materials for energy and spintronic applications. *Semicond. Sci. Technol.* **2012**, *27*, 063001. [\[CrossRef\]](#)
8. Tangirbergen, A.; Amangeldi, N.; Revankar, S.T.; Yergaliuly, G. A review of irradiation-induced hardening in FeCrAl alloy systems for accident-tolerant fuel cladding. *Nucl. Eng. Des.* **2024**, *429*, 113659. [\[CrossRef\]](#)
9. Anand, S.; Wood, M.; Xia, Y.; Wolverson, C.; Snyder, G.J. Double half-Heuslers. *Joule* **2019**, *3*, 1226–1238. [\[CrossRef\]](#)
10. Zeier, W.G.; Schmitt, J.; Hautier, G.; Aydemir, U.; Gibbs, Z.M.; Felser, C.; Snyder, G.J. Engineering half-Heusler thermoelectric materials using Zintl chemistry. *Nat. Rev. Mater.* **2016**, *1*, 16032. [\[CrossRef\]](#)
11. Rached, Y.; Caid, M.; Merabet, M.; Benalia, S.; Rached, H.; Djoudi, L.; Mokhtari, M.; Rached, D. A comprehensive computational investigations on the physical properties of TiXSb (X: Ru, Pt) half-Heusler alloys and Ti<sub>2</sub>RuPtSb<sub>2</sub> double half-Heusler. *Int. J. Quantum Chem.* **2022**, *122*, e26875. [\[CrossRef\]](#)



12. Bouhadjer, K.; Boudjelal, M.; Matougui, M.; Bentata, S.; Lantri, T.; Batouche, M.; Seddik, T.; Khenata, R.; Bouadjemi, B.; Bin Omran, S.; et al. Structural, optoelectronic, thermodynamic and thermoelectric properties of double half-Heusler (DHH)  $\text{Ti}_2\text{FeNiSb}_2$  and  $\text{Ti}_2\text{Ni}_2\text{InSb}$  compounds: A TB-mBJ study. *Chin. J. Phys.* **2023**, *85*, 508–523. [\[CrossRef\]](#)
13. Hasan, R.; Park, T.; Kim, S.; Kim, H.-S.; Jo, S.; Lee, K.H. Enhanced Thermoelectric Properties of  $\text{Ti}_2\text{FeNiSb}_2$  Double Half-Heusler Compound by Sn Doping. *Adv. Energy Sustain. Res.* **2022**, *3*, 2100206. [\[CrossRef\]](#)
14. Hassan, M.A.; El-Khouly, A.; Elsehly, E.M.; Almutib, E.N.; Elshamndy, S.K.; Serhiienko, I.; Argunov, E.V.; Sedegov, A.; Karpenkov, D.; Pashkova, D. Transport and thermoelectric properties of melt spinning synthesized  $\text{M}_2\text{FeNiSb}_2$  ( $\text{M} = \text{Ti, Hf}$ ) double half-Heusler alloys. *Mater. Res. Bull.* **2023**, *164*, 112246. [\[CrossRef\]](#)
15. Charifi, Z.; Baaziz, H.; Uğur, Ş.; Uğur, G. Prediction of the electronic structure, optical and vibrational properties of  $\text{ScXC}_2\text{Sb}_2$  ( $\text{X} = \text{V, Nb, Ta}$ ) double half-Heusler alloys: A theoretical study. *Indian J. Phys.* **2023**, *97*, 413–428. [\[CrossRef\]](#)
16. Boudjelal, M.; Bouhadjer, K.; Matougui, M.; Bentata, S.; Srivastata, V.; Bin-Omran, S.; Khenata, R. Ab initio prediction of the structural, optoelectronic, and thermoelectric properties of double half-Heusler (DHH)  $\text{ScXRh}_2\text{Bi}_2$  ( $\text{X} = \text{Nb, Ta}$ ) alloys DFT study results. *Indian J. Phys.* **2024**, *98*, 3141–3154. [\[CrossRef\]](#)
17. Mekhtiche, M.; Matougui, M.; Houari, M.; Bouadjemi, B.; Lantri, T.; Boudjelal, M.; Bentata, S. Predictive study of the new double half-Heusler compounds  $\text{Hf}_2\text{FeNiSb}_2$ ,  $\text{Nb}_2\text{Co}_2\text{GaSb}$ , and  $\text{ScNbCo}_2\text{Sb}_2$ , promising candidates for thermoelectric applications. *Indian J. Phys.* **2024**, *98*, 3121–3129. [\[CrossRef\]](#)
18. Diaf, M.; Righi, H.; Rached, H.; Rached, D.; Beddiaf, R. Ab initio study of the properties of  $\text{Ti}_2\text{PdFe (Ru) Sb}_2$  double half-Heusler semiconducting alloys. *J. Electron. Mater.* **2023**, *52*, 6514–6529. [\[CrossRef\]](#)
19. Ding, H.; Li, X.; Feng, Y.; Wu, B. Electronic structure, magnetism and disorder effect in double half-Heusler alloy  $\text{Mn}_2\text{FeCoSi}_2$ . *J. Magn. Magn. Mater.* **2022**, *555*, 169367. [\[CrossRef\]](#)
20. Douinat, O.; Boucherdoud, A.; Seghier, A.; Houari, M.; Mesbah, S.; Lantri, T.; Bestani, B. Theoretical investigation of the physical, mechanical, and thermal properties of  $\text{Zr}_2\text{XBiNi}_2$  ( $\text{X} = \text{Al, Ga}$ ) double half-Heusler alloys. *J. Mater. Res.* **2023**, *38*, 4509–4521. [\[CrossRef\]](#)
21. Berarma, K.; Essaoud, S.S.; Al Azar, S.; Al-Reyahi, A.Y.; Mousa, A.A.; Mufleh, A. Computational characterization of structural, optoelectronic, and thermoelectric properties of some double half-Heusler alloys  $\text{X}_2\text{FeY'Sb}_2$  ( $\text{X} = \text{Hf, Zr}$ ;  $\text{Y}' = \text{Ni, Pd}$ ). *Phase Transitions* **2023**, *96*, 806–821. [\[CrossRef\]](#)
22. Surucu, G.; Isik, M.; Candan, A.; Wang, X.; Gullu, H.H. Investigation of structural, electronic, magnetic, and lattice dynamical properties for  $\text{XCoBi}$  ( $\text{X} = \text{Ti, Zr, Hf}$ ) half-Heusler compounds. *Phys. B Condens. Matter* **2020**, *587*, 412146. [\[CrossRef\]](#)
23. Ma, H.; Yang, C.-L.; Wang, M.-S.; Ma, X.-G.; Yi, Y.-G. Effect of M elements ( $\text{M} = \text{Ti, Zr, and Hf}$ ) on thermoelectric performance of the half-Heusler compounds  $\text{MCoBi}$ . *J. Phys. D Appl. Phys.* **2019**, *52*, 255501. [\[CrossRef\]](#)
24. Zhu, H.; He, R.; Mao, J.; Zhu, Q.; Li, C.; Sun, J.; Ren, W.; Wang, Y.; Liu, Z.; Tang, Z.; et al. Discovery of  $\text{ZrCoBi}$  based half-Heuslers with high thermoelectric conversion efficiency. *Nat. Commun.* **2018**, *9*, 2497. [\[CrossRef\]](#)
25. Radouan, D.; Besbes, A.; Bestani, B. Investigation on electronic and thermoelectric properties of (P, As, Sb) doped  $\text{ZrCoBi}$ . *East Eur. J. Phys.* **2021**, *1*, 27–33.
26. Mekki, H.; Baaziz, H.; Charifi, Z.; Ghellab, T.; Genç, A.E.; Uğur, Ş.; Uğur, G. Properties of the double half-Heusler alloy  $\text{ScNbNi}_2\text{Sn}_2$  with respect to structural, electronic, optical, and thermoelectric aspects. *Solid State Commun.* **2023**, *363*, 115103. [\[CrossRef\]](#)
27. Saad Essaoud, S.; Bouhemadou, A.; Allali, D.; Ketfi, M.E.; Radjai, M.; Bin-Omran, S. An Ab Initio Investigation of the Structural Stability, Thermodynamic, Optoelectronic, and Thermoelectric Properties of  $\text{LuXNi}_2\text{Sn}_2$  ( $\text{X} = \text{V, Nb, Ta}$ ) Double Half Heusler Materials. *J. Inorg. Organomet. Polym.* **2024**, *34*, 885–902. [\[CrossRef\]](#)
28. Diaf, M.; Righi, H.; Beddiaf, R.; Djaballah, Y.; Rached, H. Ab initio investigation of the structural, mechanical, electronic, thermodynamic, and optical properties of  $\text{V}_2\text{FeNiGe}_2$  and  $\text{Hf}_2\text{FeNiSb}_2$  double half-Heusler compounds. *Can. J. Phys.* **2024**, *103*, 288–301. [\[CrossRef\]](#)
29. Liu, X.; Wang, S.; Dong, Z.; Chang, Y.; Zhang, J.; Zhang, X.; Luo, J. Discovery of (Sc, V)  $\text{CoSb}$  double half-Heusler alloys with low lattice thermal conductivity. *J. Alloys Compd.* **2025**, *1010*, 178078. [\[CrossRef\]](#)
30. Imasato, K.; Sauerschnig, P.; Miyata, M.; Ishida, T.; Yamamoto, A.; Ohta, M. Effects of the Fe/Ni ratio in double half-Heusler composition  $\text{HfFe}_{1-x}\text{Ni}_x\text{Sb}$ . *J. Mater. Chem. C* **2025**, *13*, 2154–2164. [\[CrossRef\]](#)
31. Kresse, G.; Furthmüller, J. Efficient iterative schemes for ab initio total-energy calculations using a plane-wave basis set. *Phys. Rev. B* **1996**, *54*, 11169–11186. [\[CrossRef\]](#) [\[PubMed\]](#)
32. Kresse, G.; Furthmüller, J. Efficiency of ab-initio total energy calculations for metals and semiconductors using a plane-wave basis set. *Comput. Mater. Sci.* **1996**, *6*, 15–50. [\[CrossRef\]](#)
33. Mastrikov, Y.A.; Chuklina, N.G.; Sokolov, M.N.; Popov, A.I.; Gryaznov, D.V.; Kotomin, E.A.; Maier, J. Small radius electron and hole polarons in  $\text{PbX}_2$  ( $\text{X} = \text{F, Cl, Br}$ ) crystals: A computational study. *J. Mater. Chem. C* **2021**, *9*, 16536–16544. [\[CrossRef\]](#)



34. Mastrikov, Y.A.; Gryaznov, D.; Sokolov, M.N.; Zvejnieks, G.; Popov, A.I.; Eglitis, R.I.; Kotomin, E.A.; Ananyev, M.V. Oxygen Vacancy Formation and Migration within the Antiphase Boundaries in Lanthanum Scandate-Based Oxides: Computational Study. *Materials* **2022**, *15*, 2695. [\[CrossRef\]](#)
35. Kaptagay, G.A.; Satanova, B.M.; Abuova, A.U.; Konuhova, M.; Zakiyeva, Z.Y.; Tolegen, U.Z.; Koilyk, N.O.; Abuova, F.U. Effect of rhodium doping for photocatalytic activity of barium titanate. *Opt. Mater. X* **2025**, *25*, 100382. [\[CrossRef\]](#)
36. Inerbaev, T.M.; Abuova, A.U.; Zakiyeva, Z.Y.; Abuova, F.U.; Mastrikov, Y.A.; Sokolov, M.; Gryaznov, D.; Kotomin, E.A. Effect of Rh doping on optical absorption and oxygen evolution reaction activity on BaTiO<sub>3</sub> (001) surfaces. *Molecules* **2024**, *29*, 2707. [\[CrossRef\]](#)
37. Inerbaev, T.M.; Graupner, D.R.; Abuova, A.U.; Abuova, F.U.; Kilin, D.S. Optical properties of BaTiO<sub>3</sub> at room temperature: DFT modelling. *RSC Adv.* **2025**, *15*, 5405–5412. [\[CrossRef\]](#)
38. Perdew, J.P.; Burke, K.; Ernzerhof, M. Generalized gradient approximation made simple. *Phys. Rev. Lett.* **1996**, *77*, 3865. [\[CrossRef\]](#)
39. Togo, A.; Tanaka, I. First principles phonon calculations in materials science. *Scr. Mater.* **2015**, *108*, 1–5. [\[CrossRef\]](#)
40. Fan, T.; Oganov, A.R. AICON: A program for calculating thermal conductivity quickly and accurately. *Comput. Phys. Commun.* **2020**, *251*, 107074. [\[CrossRef\]](#)
41. Anand, S.; Xia, K.; Hegde, V.I.; Aydemir, U.; Kocovski, V.; Zhu, T.; Wolverton, C.; Snyder, G.J. A valence balanced rule for discovery of 18-electron half-Heuslers with defects. *Energy Environ. Sci.* **2018**, *11*, 1480–1488. [\[CrossRef\]](#)
42. Mouhat, F.; Coudert, F.-X. Necessary and sufficient elastic stability conditions in various crystal systems. *Phys. Rev. B* **2014**, *90*, 224104. [\[CrossRef\]](#)
43. Voigt, W. *Lehrbuch der Kristallphysik (Textbook of Crystal Physics)*; BG Teubner: Leipzig, Germany; Berlin, Germany, 1928.
44. Reuss, A.J.Z. Calculation of the flow limits of mixed crystals on the basis of the plasticity of monocrystals. *Z. Angew. Math. Mech.* **1929**, *9*, 49–58. [\[CrossRef\]](#)
45. Hill, R. The elastic behaviour of a crystalline aggregate. *Proc. Phys. Soc. A* **1952**, *65*, 349. [\[CrossRef\]](#)
46. Hill, R. Elastic properties of reinforced solids: Some theoretical principles. *J. Mech. Phys. Solids* **1963**, *11*, 357–372. [\[CrossRef\]](#)
47. Chen, H.; Yang, L.; Long, J. First-principles investigation of the elastic, Vickers hardness, and thermodynamic properties of Al–Cu intermetallic compounds. *Superlattices Microstruct.* **2015**, *79*, 156–165. [\[CrossRef\]](#)
48. Frantsevich, I.N. Elastic constants and elastic moduli of metals and insulators. In *Reference Book*; Naukova Dumka: Kyiv, Ukraine, 1982.
49. Ranganathan, S.I.; Ostoja-Starzewski, M. Universal elastic anisotropy index. *Phys. Rev. Lett.* **2008**, *101*, 055504. [\[CrossRef\]](#)
50. Chen, X.-Q.; Niu, H.; Li, D.; Li, Y. Modeling hardness of polycrystalline materials and bulk metallic glasses. *Intermetallics* **2011**, *19*, 1275–1281. [\[CrossRef\]](#)
51. Tian, Y.; Xu, B.; Zhao, Z. Microscopic theory of hardness and design of novel superhard crystals. *Int. J. Refract. Met. Hard Mater.* **2012**, *33*, 93–106. [\[CrossRef\]](#)
52. Niu, H.; Niu, S.; Oganov, A.R. Simple and accurate model of fracture toughness of solids. *J. Appl. Phys.* **2019**, *125*, 6. [\[CrossRef\]](#)
53. Thompson, R.P.; Clegg, W.J. Predicting whether a material is ductile or brittle. *Curr. Opin. Solid State Mater. Sci.* **2018**, *22*, 3–100. [\[CrossRef\]](#)
54. Dasmahapatra, A.; Daga, L.E.; Karttunen, A.J.; Maschio, L.; Casassa, S. Key role of defects in thermoelectric performance of TiMnSn (M = Ni, Pd, and Pt) half-Heusler alloys. *J. Phys. Chem. C* **2020**, *124*, 14997–15006. [\[CrossRef\]](#)
55. Xiao, Y.; Zhao, L.-D. Charge and phonon transport in PbTe-based thermoelectric materials. *npj Quantum Mater.* **2018**, *3*, 55. [\[CrossRef\]](#)
56. Zhai, J.; Wang, T.; Wang, H.; Su, W.; Wang, X.; Chen, T.; Wang, C. Strategies for optimizing the thermoelectricity of PbTe alloys. *Chin. Phys. B* **2018**, *27*, 047306. [\[CrossRef\]](#)
57. Xi, J.; Dong, Z.; Gao, M.; Luo, J.; Yang, J. Screening of half-Heuslers with temperature-induced band convergence and enhanced thermoelectric properties. *arXiv* **2024**, arXiv:2407.00433.
58. Krukau, A.V.; Vydrov, O.A.; Izmaylov, A.F.; Scuseria, G.E. Influence of the exchange screening parameter on the performance of screened hybrid functionals. *J. Phys. Chem. C* **2006**, *125*, 224106. [\[CrossRef\]](#)
59. Gautier, R.; Zhang, X.; Hu, L.; Yu, L.; Lin, Y.; Sunde, T.O.L.; Chon, D.; Poepplmeier, K.R.; Zunger, A. Prediction and accelerated laboratory discovery of previously unknown 18-electron ABX compounds. *Nat. Chem.* **2015**, *7*, 308–316. [\[CrossRef\]](#)

**Disclaimer/Publisher’s Note:** The statements, opinions and data contained in all publications are solely those of the individual author(s) and contributor(s) and not of MDPI and/or the editor(s). MDPI and/or the editor(s) disclaim responsibility for any injury to people or property resulting from any ideas, methods, instructions or products referred to in the content.